Current Similarity Analysis-Based Open-Circuit Fault Diagnosis for Two-Level Three-Phase PWM Rectifier

Feng Wu, *Student Member, IEEE*, and Jin Zhao, *Senior Member, IEEE*

***Abstract*—This paper proposed a novel single and multiple transistors open-circuit fault diagnosis method for two-level three-phase pulse-width modulating rectifier based on topology symmetry analysis in healthy and faulty conditions. First, similarity measurements between any two phase current linklists contained samples in a period after reconstruction and shape analysis, such as Euclidean distance, correlation coefficient, and cosine angle, are used to describe the symmetry of topology and divide the faults into three classes, then two extra features are extracted to locate the fault to broken leg and transistors, respectively. The proposed diagnostic method is robust, low cost, and easy to insert to the existed control system. The effectiveness and merit were evaluated by experimental results.**

***Index Terms*—Currents data reconstruction, fault diagnosis, open circuit, pulse-width modulating (PWM) rectifier, similarity measurements.**

NOMENCLATURE

CDR	Current Data Reconstruction
CSA	Current Shape Analysis
SM	Similarity Measurement
ED	Euclidean Distance
CC	Correlation Coefficient
CA	Cosine Angle
FD	Diagnostic Signal, Fault Detection
FI	Diagnostic Signal, Fault Location
CL	Current Linklist Contained Samples in a Period
ZCS	Zero-Crossing Sample
m	Representative of a,b,c
$i_m(k)$	Current Sample in k instant
$U_d{}^*$	Reference Output Voltage
U_d	Output Voltage
f_s	Primary Source Frequency
$T_{\rm sp}$	Current Sampling Period
L	Number of Current Samples in a Period
k	Sampling instant
t	$k-L+1$
p_1	Position of Down-to-Up ZCS
p_2	Position of Up-to-Down ZCS
I_m	Original CLs
$\hat{I}_m$	Reconstructed CLs
D_m	Difference between Two Nearby Samples
$\hat{D}_m$	CLs after CSA
$d_{\rm mn}$	Value of ED between $\hat{D}_m$, $\hat{D}_n$
$\rho_{\rm mn}$	Value of CC between $\hat{D}_m$, $\hat{D}_n$
$\psi_{\rm mn}$	Value of CA between $\hat{D}_m$, $\hat{D}_n$
M_m	Percentage of Close-to-Zero Samples
S_m	Polar of Phase Current
N_1, N_2	Filters constant
k_ξ	Parameter, Criterion for Close-to-Zero Sample
k_z	Parameter, Criterion for Broken Leg
$k_{\rm sim1}$	Parameter, Criterion for Simialrity of CC/CA
$k_{\rm sim2}$	Parameter, Criterion for Simialrity of ED

Manuscript received January 22, 2016; revised May 24, 2016; accepted June 28, 2016. Date of publication July 7, 2016; date of current version February 2, 2017. This work was supported by the National Natural Science Foundation of China under Grants 61273174 and 61573159. Recommended for publication by Associate Editor S. Choi.

The authors are with the Key Laboratory of Image Information Processing and Intelligent Control, Ministry of Education, and the School of Automation, Huazhong University of Science and Technology, Wuhan 430074, China (e-mail: wf199010202051@163.com; jinzhao617@163.com).

Color versions of one or more of the figures in this paper are available online at http://ieeexplore.ieee.org.

Digital Object Identifier 10.1109/TPEL.2016.2587339

I. INTRODUCTION

THREE-PHASE pulse-width modulating (PWM) rectifiers are widely used in industrial applications such as renewable energy, high power electrolysis, and electroplate. PWM rectifiers have many advantages compared to the conventional diode or thysistor rectifiers, such as stabilization and regulation of dc link voltage (current), lower harmonic distortion of line current, bidirection power flow from the primary source to load, and back from load to the source [1]. The last characteristic is very important for application of the rectifiers in electric drives. Today, two basic rectifier topologies are widely accepted, boost rectifier with voltage output and buck rectifier with current output. Generally, completely controlled transistors are used as switching components, such as insulated-gate bipolar transistors (IGBTs), and MOSFETs. The healthy condition of the semiconductor is one of the most important factors that will affect the reliability and efficiency of a system. Power converters are complex devices that are often exposed to high stresses, being therefore very prone to suffer critical failures [2]. Reports and surveys estimate that about 38% of the faults in power conversion system are due to failures in power devices such as IGBTs. Recent surveys show that the failure rate of semiconductor power device reduces, as the most fragile component, their failure rate is 31%, which follows by "capacitors" and "gate drives" [3]–[5]. The strong reliability demand of power device makes the development of fault diagnosis methods become a hotspot during the last years [6]–[9].

Generally, semiconductor switch device faults in power converters are subdivided into short circuit and open circuit. Short circuit of these elements in most cases causes an overcurrent, which is very destructive and makes the drive system shut down immediately. Nowadays, short-circuit fault detection has become a standard feature of drives hardware, few research results are published on them. However, open circuit does not immediately cause the system shutdown and can remain undetected for an extended period of time [10], this can lead to overstress on the healthy switches and in turn cause second failures in other components, as well as lead to a ripple outputs. As a result, the system will be shut down by the subsequent faults and needs higher repairing cost [11], [12].

Therefore, it is essential to develop lots of fault diagnosis methods to improve the reliability of converters. As is known to all, open-circuit fault diagnosis in power converters includes fault detection and fault isolation/location. Usually, fault detection requires antitransients ability to avoid false alarms, fault isolation requires efficiency, and accuracy to identify fault types. In most cases, they are studied together.

Fair robustness, fast detection time, and effective location can be achieved in some voltage-based methods [13]–[15] at the cost of extra voltage sensors or electrical circuits. The major disadvantages of these approaches are the use of at least two additional voltage sensors or electrical circuits, which brings uncertainty and increases the cost of the drives.

Nowadays, lots of researchers pay attention to current-based fault diagnosis for low cost and independence to control system. In two-level three-phase voltage-source inverter (VSI), the Park's vector approach was first proposed in [16] as a fault diagnostic tool. This method is not suitable for integration into the drive controller due to its poor robustness and complex implementation. Normalized dc current methods are proposed in [17] and [18], these methods have a major drawback of being load dependant and inapplicable to a closed-loop control scheme. Model-based methods are proposed in [19]–[21], these methods are effective, fast and low cost, however, they are poor in robustness and sensitive to parameters. Recently, load current analysis method, current sections analysis in dq-coordinate, and symmetry analysis based on allelic points are proposed in [22]–[24], these methods perform well in fault detection for their fair robustness to variable load and speed, as well as effective and accurate fault location.

Failures in matrix converter and multilevel inverters are also focused lots of research work. Fast and low cost fault detection and location for matrix converter are proposed in [25] based on an electrical circuit analysis. A fault diagnostic method [26] on the basis of the radius of the concordia current pattern is proposed for grid-connected neutral-point-clamped inverter system. Method based on a normalized average phase current and a negative reactive current injection is proposed in [27] for fault detection in T-type three-level inverter system. Lots of currents-based methods are proposed in [8] and [28] for multilevel converter. Dynamic current–voltage characteristics are used in [29] for fault diagnosis of photovoltaic panels. All the research work mentioned above focus on the fault location, little publication is related to antitransient fault detection.

Although open-circuit fault has been a hotspot in the past decades, most publications concern about inverters, However, the portability to rectifier is poor for the operation principles of VSI and rectifier are different. Hence, it is necessary to carry out research works on the rectifier. In [30], the instant converter voltage error is used for failure analysis in three-level neutral-point-clamped boost rectifier, it can detect and identify faults when the line current in the affected phase is reduced to zero. In [31], mixed logical dynamic model and generated residual are used for open-circuit fault diagnosis in a single-phase rectifier. In two-level three-phase rectifier, in [32], an open-switch fault diagnosis method by considering the switching patterns of space vector PWM and the directions of faulty phase current are proposed, however, its antitransients ability is poor. In [33], differences between open circuit in inverter and rectifier are analyzed, modifying Park's vector method and normalized dc current method are used for fault diagnosis. In [34], a combination of the absolute normalized dc current method is proposed. It should be noted that the study of two-level three-phase rectifier fault diagnosis is little, what's more, the methods-mentioned above only relate to a single open-circuit fault diagnosis.

In this paper, fair-robust fault detection and location methods for single and multiple open-circuit faults in two-level three-phase rectifier are proposed. The major contributions are made as following:

1) distances between any two phase CLs after CSA are applied to measure their similarity, which indicates the symmetry of two corresponding legs, based on the value of similarity, a fairly robust fault detection is proposed;
2) the proposed fault location method can identify both single and multiple open-circuit faults;
3) comprehensive performance of the proposed method is more superior than the previous methods.

The structure of this paper is as following, Section II introduces the three-phase rectifier with fault diagnosis scheme. Section III expounds the proposed dynamic CDR, CSA, SMs, fault detection and location method, including tuning efforts. Section IV is the experimental results and the performance comparison with previous methods. A conclusion is summarized in Section V.

II. Structure of Two-Level Three-Phase Rectifier

The structure of three-phase rectifier with proposed fault diagnostic unit is depicted in Fig. 1. It contains three-phase primary source voltages (u_a, u_b, u_c), three-phase primary inductances $(L_{\rm as}, L_{\rm bs}, L_{\rm cs})$, six transistors (T1, T2, T3, T4, T5, T6) equipped with six diodes $(\mathrm{D1}, \mathrm{D2}, \mathrm{D3}, \mathrm{D4}, \mathrm{D5}, \mathrm{D6})$, respectively, rectifier control system with a unity power factor, capacitor filter $(C1, C2)$ with resistance load R_L, and fault diagnosis unit. Three-phase current (i_a, i_b, i_c), the predefined dc values $({U_d}^*)$, the measured dc values (U_d) are used as inputs of control system to generate drive signals to control the transistors ON and OFF, alternatively. Here, in the proposed method, three-phase currents are first pretreated by CDR and CSA, then distances between any two pretreated phase currents are applied to measure the similarity between them, which indicates the

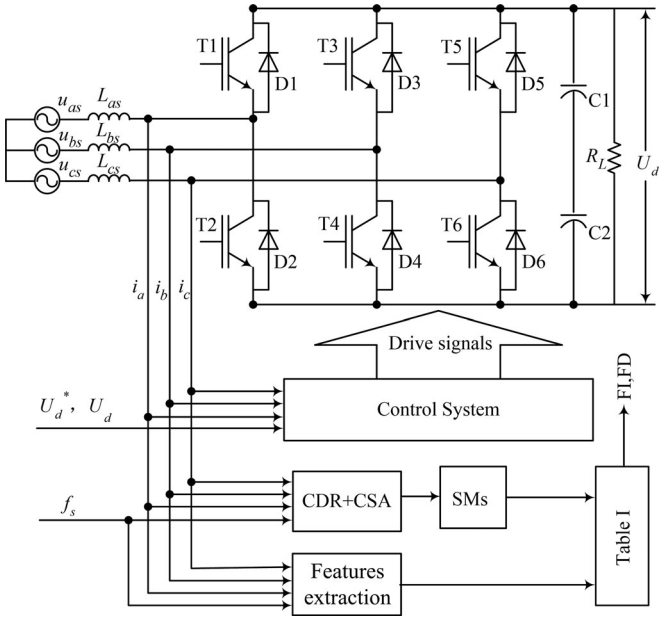

Fig. 1. Structure of two-level three-phase rectifier with proposed fault diagnosis unit.

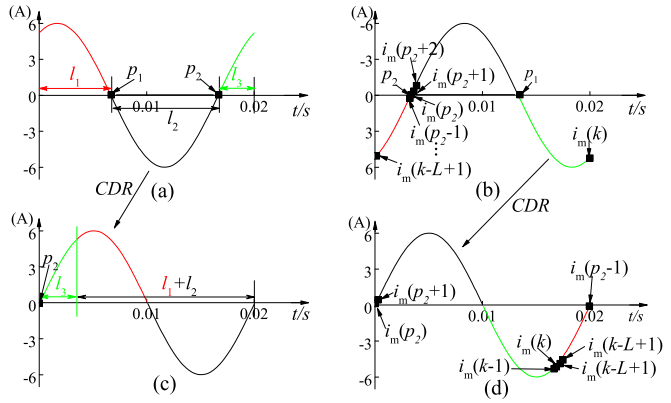

Fig. 2. Current waveforms before and after CDR, (a) original current waveform, (b) original current samples, (c) reconstructed current waveform, and (d) reconstructed current samples.

symmetry of three legs in topology. According to the similarity, fault can be detected, meanwhile, 21 open-circuit faults can be divided into three classes. Then, the faulty transistors can be located combined with two extra features. FD and FI are the two diagnostic signals that show the results of fault detection and location, respectively.

III. Proposed Fault Diagnosis Method

Symmetrical topology with the same components or devices is a classical characteristics of power electronic systems, such as three-phase inverters or rectifiers, matrix, and multilevel converters. The symmetry will change when the system drops from a healthy condition to a faulty condition. Wu and Zhao [24] tries to use three-phase currents to describe the symmetry in three-phase VSI fed induction motor both in healthy and faulty conditions, however, the proposed method lacks of widely recognized theory and is inapplicable to two-level three-phase rectifier. In this paper, distances between any two phase currents, such as ED, CC, and CA, are used to measure their similarity, which is corresponding to the symmetry of the topology. Based on symmetry analysis in healthy and faulty conditions, a fault detection and location method is proposed in this paper. Considering three-phase original currents are ruleless, current pretreated algorithms including CDR and CSA are proposed for a understandable similarity measurement.

A. Current Data Reconstruction

For a periodic signal, feature in a period can represent all the signal characteristics according to self-similar theory [35]. Three-phase currents in PWM rectifier are periodic under healthy and faulty conditions. Here, sliding windows contained current samples in a period are named after CLs. The length of CLs L is given as

$$L = \frac{1}{f_s} T_{\mathrm{sp}}. \tag{1}$$

At k instant, t is defined as

$$t = k - L + 1. \tag{2}$$

Three original CLs are showed as the following:

$$I_m(k) = [i_m(t), i_m(t+1), \ldots, i_m(k)]. \tag{3}$$

At every instant, three phase CLs are updated by abandoning the oldest samples and adding the new samples. At $k+1$ instant, there is

$$I_m(k+1) = [i_m(t+1), i_m(t+2), \ldots, i_m(k+1)]. \tag{4}$$

Phase difference exists between any two CLs both in healthy and faulty conditions. The phase difference in healthy condition is constant with $2\pi/3$. While the phase difference in different faulty condition is variable, such as the phase difference between phase-b and phase-c is π when T1T2 fail. In order to eliminate the influence of phase difference on SM. A dynamic current data reconstruction algorithm is proposed by reconstructing the CLs to the same coordinate origin. Fig. 2(a) and (b) shows the original CLs. Two ZCSs $i_m(p_1)$, $i_m(p_2)$ divide the CLs into several parts, such as l_1, l_2, and l_3 in Fig. 3(a). Especially, l_1 is equal to zero when p_1 is the first position of the CL, l_3 is equal to zero when p_2 is the first position of the CL. In the proposed CDR algorithm, p_1 or p_2 is set as leading position, the current samples before p_1 or p_2 are removed strictly to the ending position of the original linklists to form reconstructed CLs, showed as (5). Fig. 3(a) and (c) shows the process of CDR in time series, p_2 is set as leading position, waveforms l_1, l_2 before p_2 are strictly removed to the ending position of original waveforms. Fig. 3(b) and (d) shows the process of CDR in a discrete system.

$$\begin{aligned} \hat{I}_m(k) = [&i_m(p_v), i_m(p_v+1), \ldots, \\ &i_m(k), i_m(t), i_m(t+1), \ldots, i_m(p_v-1)] \\ &v = 1, 2. \end{aligned} \tag{5}$$

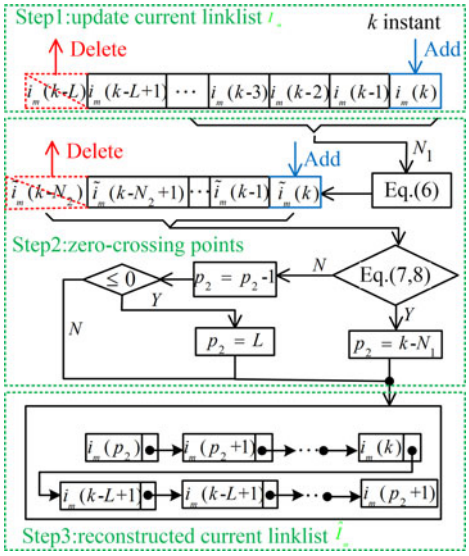

Fig. 3. Algorithm flowchart of CDR with down-to-up ZCS p_2 as heading position.

Current harmonics and system noise may cause fluctuation near zero, which has a negative influence on the calculation of ZCS. Here, two filters are designed. The first one is a mean value filter, showed as (6), where N_1 is a counter

$$\widetilde{i}_m(k) = \frac{1}{N_1}(i_m(k) + i_m(k-1) + \cdots i_m(k-N_1+1)). \tag{6}$$

Meanwhile, the second filter is designed to avoid false calculation caused by closed-to-zero ac nodes, for $j = k - N_2$ $\forall v \in [k-N_2+1, k-N_2+2, \ldots, k]$, if

$$\begin{cases} \widetilde{i}_m(j) < 0 \\ \widetilde{i}_m(v) \geq 0. \end{cases} \tag{7}$$

Then, $p_2 = k - N_2$; for $j = k$ $\forall v \in [k-N_2, k-N_2+1, \ldots, k-1]$, if

$$\begin{cases} \widetilde{i}_m(j) > 0 \\ \widetilde{i}_m(v) \leq 0. \end{cases} \tag{8}$$

Then, $P_1 = k - N_2$. At k instant, if (7) or (8) is workable, position of ZCS will be replaced by $k - N_2$, otherwise, position of ZCS will shift left during CLs update.

Consequently, three-phase reconstructed CLs are presented as (9), phase differences between any two of them are eliminated

$$\begin{bmatrix} \hat{I}_a(k) \\ -\hat{I}_b(k) \\ \hat{I}_c(k) \end{bmatrix} = \begin{bmatrix} i_a(p_2) \cdots i_a(k)\ i_a(t) \cdots i_a(p_2-1) \\ i_b(p_1) \cdots i_b(k)\ i_b(t) \cdots i_b(p_1-1) \\ i_c(p_2) \cdots i_c(k)\ i_c(t) \cdots i_c(p_2-1) \end{bmatrix}. \tag{9}$$

Fig. 3 shows the algorithm flowchart of CDR with $i_m(p_2)$ as leading position. It includes three steps:

1) update CLs;
2) calculate the position of ZCS;
3) form the reconstructed CLs.

Subfigure 1 of Fig. 4(a)–(d) showed the original CLs generated from experimental board, subfigure 2 of Fig. 4(a)–(d) showed the reconstructed CLs when T1, T1T2, T1T3, T1T4 fail, respectively. Intuitively, faulty characteristics are more obvious after CDR. The most important contribution is that the reconstructed CLs are nearly all the same at every instant, which facilitates SM with the distance between any two of them.

B. Current Shape Analysis

Traditional SMs in signal processing, such as ED, CC, and CA, are sensitive to shifting, scaling, and time warpings [36]–[38], these exist in reconstructed CLs when an open-circuit fault occurs. Practically, obvious shifting and scaling exist in CLs between phase-b and phase-c when T1 fails, showed as subfigure 2 in Fig. 4(a). Little scaling exists between CLs of phase-b and phase-c when both T1 and T2 fail, showed as subfigure 2 in Fig. 4(b). Extreme shifting, scaling, and warps in temporal dimension exist between CLs of phase-a and phase-b when both T1 and T3 fail, showed as subfigure 2 in Fig. 4(c). Obvious warps in temporal dimension in the second half period and extreme scaling exist between CLs of phase-a and phase-b when both T1 and T4 fail, showed as subfigure 2 in Fig. 4(d). In this paper, derivative-based CSA is proposed to handle these problems. Here supposing there are two time series y_1, y_2, showed as in (10), where $A_1 \neq A_2$, d represents the scaling value, B represents the shifting value

$$\begin{cases} y_1 = A_1 f(t) \\ y_2 = A_2 f(t) + B \\ d = \frac{A_1}{A_2}. \end{cases} \tag{10}$$

The derivative of y_1,y_2 are linear correlation, showed as

$$\frac{\partial y_1}{\partial y_2} = \frac{A_1 \partial f}{A_2 \partial f} = d. \tag{11}$$

In discrete system, derivative is expressed by difference function, given as

$$\frac{\partial y}{\partial t} = \frac{y(k) - y(k-1)}{T_{\text{sp}}}. \tag{12}$$

Considering T_{sp} is a constant, derivative of reconstructed CLs can be expressed as

$$D_m(k) = \hat{I}_m(k) - \hat{I}_m(k-1). \tag{13}$$

Time warping is another factor that affects SM. Fortunately, time warpings of reconstructed CLs are in x-axis. It can be eliminated by mapping and sorting the waveforms to the warping dimension. The distances of the current waveforms to the warping dimension are the absolute value of current samples. Elements of D_m are replaced by its absolute value and sorted from small to large to form new CLs $\hat{D}_m$. Subfigure 3 of Fig. 4(a)–(d) showed the results CLs after CSA of four typical faults T1, T1T2, T1T3, and T1T4, respectively.

C. Similarity Measurements

Distances between any two CLs after CSA are used to measure the similarity between them, which represents the

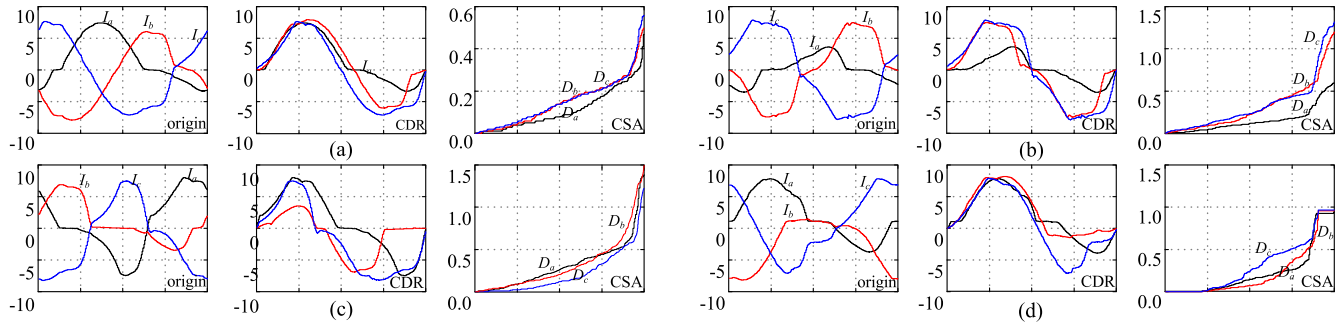

Fig. 4. Three-phase CLs of four typical faults. (a) T1 fails. (b) T1T2 fail. (c) T1T3 fail. (d) T1T4 fail. From left to right, Subplot 1: original CLs. Subplot 2: reconstructed CLs. Subplot 3: CLs after CSA.

symmetry between the corresponding legs. In this paper, three different SMs are investigated.

CLs can be seen as a time series with same length, which can be expressed as $\hat{D}_m[d_m(1), d_m(2), \ldots, d_m(L)]$ and $\hat{D}_n[d_n(1), d_n(2), \ldots, d_n(L)]$, where $m, n = a, b, c; m \neq n$. ED is a general SM method for time series with same length, as (14), where $d_{\mathrm{mn}}(\hat{D}_m, \hat{D}_n)$ is the Euclidean distance of the two CLs $\hat{D}_m$ and $\hat{D}_n$. The smaller value for $d_{\mathrm{mn}}(\hat{D}_m, \hat{D}_n)$ indicates they are close and more similar, the larger value for $d_{\mathrm{mn}}(\hat{D}_m, \hat{D}_n)$ indicates they are distant and less similar

$$d_{\mathrm{mn}}(\hat{D}_m, \hat{D}_n) = \left(\sum_{k=1}^{L} |d_m(k) - d_n(k)|^2 \right)^{1/2}. \tag{14}$$

CLs can be seen as samples in statistic theory, covariation, and CC of two samples $\hat{D}_m[d_m(1), d_m(2), \ldots, d_m(L)]$ and $\hat{D}_n[d_n(1), d_n(2), \ldots, d_n(L)]$ are applied to SM, as (15), where $\rho_{\mathrm{mn}}(\hat{D}_m, \hat{D}_n)$ is the correlation coefficients of $\hat{D}_m$ and $\hat{D}_n$, and $\rho_{\mathrm{mn}}(\hat{D}_m, \hat{D}_n) \in [0, 1]$, $\bar{D}_m$,$\bar{D}_n$ are the mean value of $\hat{D}_m$ and $\hat{D}_n$. The value of 1 for $\rho_{\mathrm{mn}}(\hat{D}_m, \hat{D}_n)$ indicates perfect linear correlation; the value of 0 indicates no linear correlation at all. Obviously, a larger value of $\rho_{\mathrm{mn}}(\hat{D}_m, \hat{D}_n)$ for two samples indicates more correlation and similarity between them

$$\rho_{\mathrm{mn}}(\hat{D}_m, \hat{D}_n) = \frac{\sum_{k=1}^{L} \left| (\hat{d}_m(k) - \bar{D}_m)(\hat{d}_n(k) - \bar{D}_n) \right|}{\sqrt{(\sum_{k=1}^{L} (\hat{d}_m(k) - \bar{D}_m)^2)(\sum_{k=1}^{L} (\hat{d}_n(k) - \bar{D}_n)^2)}}$$

$$\bar{D}_m = \frac{1}{L} \sum_{k=1}^{L} \hat{d}_m(k)$$

$$\bar{D}_n = \frac{1}{L} \sum_{k=1}^{L} \hat{d}_n(k). \tag{15}$$

CLs can be also seen as vectors, CA of vectors $\hat{D}_m$ $[d_m(1), d_m(2), \ldots, i_d(L)]$ and $\hat{D}_n[d_n(1), d_n(2), \ldots, d_n(L)]$ also can be applied to SM, as (16), it represents the similarity of two vectors directions, where $\psi_{\mathrm{mn}}(\hat{D}_m, \hat{D}_n)$ is the cosine angle of $\hat{D}_m$ and $\hat{D}_n$, and $\psi_{\mathrm{mn}}(\hat{D}_m, \hat{D}_n) \in [0, 1]$. The value of 1 for $\psi_{\mathrm{mn}}(\hat{D}_m, \hat{D}_n)$ indicates two vectors are in the same or opposite direction, the value of 0 for $\psi_{\mathrm{mn}}(\hat{D}_m, \hat{D}_n)$ indicates two vectors are in orthogonal direction. Obviously, a larger value of $\psi_{\mathrm{mn}}(\hat{D}_m, \hat{D}_n)$ for two vectors indicates more similarity between them

$$\psi_{\mathrm{mn}}(\hat{D}_m, \hat{D}_n) = \frac{\left| \sum_{k=1}^{L} d_m(k) \cdot d_n(k) \right|}{\sqrt{\sum_{k=1}^{L} {d_m}^2(k) \cdot \sum_{k=1}^{L} {d_n}^2(k)}}. \tag{16}$$

D. Proposed Fault Diagnosis Method

1) Fault Detection: Values of SMs are used to measure the similarity between any two CLs, which represents the symmetry of the topology. In healthy condition, all three legs are symmetrical, distance between any two CLs is small, all three CLs are similar. When fault occurs, this does not establish. Thresholds used to qualitative analysis of symmetry are defined as (19), where $\sim$ means the left is symmetric with the right. The criterion for symmetry is different when different SM is used. For CA and CC, the value of ρ_{mn} or ψ_{mn} represents that CLs of phase-m and phase-n are similar if it is larger than K_{sim1}, which indicates leg-m and leg-n are symmetrical. For ED, the value of d_{mn} represents that leg-m and leg-n are symmetrical if it is smaller than K_{sim2}

$$\begin{cases} \rho_{\mathrm{mn}} > K_{\mathrm{sim1}} \Leftrightarrow \text{leg-}m \sim \text{leg-}n \\ \psi_{\mathrm{mn}} > K_{\mathrm{sim1}} \Leftrightarrow \text{leg-}m \sim \text{leg-}n \\ d_{\mathrm{mn}} < K_{\mathrm{sim2}} \Leftrightarrow \text{leg-}m \sim \text{leg-}n. \end{cases} \tag{17}$$

As a result, criterion of fault detection can be presented as

$$\mathrm{FD} = \begin{cases} & \rho_{\mathrm{ab}}, \rho_{\mathrm{bc}}, \rho_{\mathrm{ac}} > K_{\mathrm{sim1}} \\ 0, & \psi_{\mathrm{ab}}, \psi_{\mathrm{bc}}, \psi_{\mathrm{ac}} > K_{\mathrm{sim1}} \\ & d_{\mathrm{ab}}, d_{\mathrm{bc}}, d_{\mathrm{ac}} < K_{\mathrm{sim2}} \\ 1, & \text{else.} \end{cases} \tag{18}$$

Taking CC and CA for example, if all three values of SMs are larger than predefined thresholds K_{sim1}, all three phase CLs after CSA are similar, which indicates three legs are symmetric, the system is healthy. Otherwise, the symmetry of rectifier will be broken, which indicate fault occurrence.

2) Fault Location: Transistor open-circuit fault will break the symmetry of the system topology. Only two legs are symmetrical in faulty condition. Twenty-one open-circuit faults are first divided to three classes FAULT_1, FAULT_2, and FAULT_3, respectively, according to the similarity of CLs after CSA, showed

TABLE I
PROPOSED FAULT DIAGNOSIS TABLE WITH ED

Healthy Condition	SMs	Features		Faulty Transistors	Fault Type
		M_m	S_m		
Healthy	$d_{\rm ab}, d_{\rm bc}, d_{\rm ac} < K_{\rm sim2}$	×	×	×	0
		$M_a > K_z$	$S_a = 0$	T1T2	1
			$S_a > 0$	T1	2
			$S_a < 0$	T2	3
Fault_1	$d_{\rm bc} < K_{\rm sim2} d_{\rm ab}$, $d_{\rm ac} > K_{\rm sim2}$	$(M_b > K_z) \wedge (M_c > K_z)$	$S_b > 0, S_c > 0$	T3T5	4
			$S_b < 0, S_c < 0$	T4T6	5
			$S_b > 0, S_c < 0$	T3T6	6
			$S_b < 0, S_c > 0$	T4T5	7
		$M_b > K_z$	$S_b = 0$	T3T4	8
			$S_b > 0$	T3	9
			$S_b < 0$	T4	10
Fault_2	$d_{\rm ac} < K_{\rm sim2} d_{\rm ab}$, $d_{\rm bc} > K_{\rm sim2}$	$(M_a > K_z) \wedge (M_c > K_z)$	$S_a > 0, S_c > 0$	T1T5	11
			$S_a < 0, S_c < 0$	T2T6	12
			$S_a > 0, S_c < 0$	T1T6	13
			$S_a < 0, S_c > 0$	T2T5	14
		$M_a > K_z$	$S_c = 0$	T5T6	15
			$S_c > 0$	T5	16
			$S_c < 0$	T6	17
Fault_3	$d_{\rm ab} < K_{\rm sim2} d_{\rm ac}$, $d_{\rm bc} < K_{\rm sim2}$	$(M_a > K_z) \wedge (M_b > K_z)$	$S_a > 0, S_b > 0$	T1T3	18
			$S_a < 0, S_b < 0$	T2T4	19
			$S_a > 0, S_b < 0$	T1T4	20
			$S_a < 0, S_b > 0$	T2T3	21

in Table I. Every fault class results from two faulty conditions, taking FAULT_1 as example, the relationships of SMs are $d_{\rm bc} < K_{\rm sim2}, d_{\rm ab}, d_{\rm ac} > K_{\rm sim2}$ or $\rho_{\rm bc} > K_{\rm sim1}, \rho_{\rm ab}, \rho_{\rm ac} < K_{\rm sim1}$ or $\psi_{\rm bc} > K_{\rm sim1}, \psi_{\rm ab}, \psi_{\rm ac} < K_{\rm sim1}$, leg-$b$ and leg-c are symmetrical, leg-a is asymmetrical with them. It may be caused by that only leg-a is broken or both leg-b and leg$c$ are broken. If leg-a is broken, then the faulty transistor may be T1, T2 or T1T2. If both leg-b and leg-c are broken, the broken transistor may be T1T3, T2T4, T1T4 or T2T3. In order to identify the faulty transistor from FAULT_1, extra diagnostic features are designed.

When transistor open circuit occurs, the connected diode will continue operating by replacing the faulty transistor to realize energy conversion. Diode conduction drop is set as U_D, when the voltage drop of diode is smaller than U_D, the connected diode will be nonconducted, leading to a short closed-to-zero intervals in the corresponding phase current. When the voltage drop of diode is larger than U_D, diode will be conducted. The closed-to-zero current samples at k instant can be defined as (21). K_ξ is a predefined minimal threshold, $H_m = 1$ represents that $i_m(k)$ is close-to-zero

$$H_m(k) = \begin{cases} 1, & |i_m(k)| < K_\xi \\ 0, & \text{else.} \end{cases} \tag{19}$$

The percentage of closed-to-zero current samples in a period can be expressed as following:

$$M_m(k) = \frac{1}{L} \sum_{j=t}^{k} H_m(j). \tag{20}$$

In FAULT_1, if M_a is larger than a predefined threshold K_z, then leg-a is broken, if M_b or M_c is larger than K_z, then there is a faulty transistor in leg-b and leg-c, respectively.

Here, another feature is applied to identify whether the broken transistor is on the upper or on the lower or both of them, giving as (23). S_m is defined as a ratio of the sum to absolute sum of current samples in a period. It represents the energy polar flowed through leg-m

$$S_m(k) = \frac{\sum_{j=t}^{k} i_m(j)}{|\sum_{j=t}^{k} i_m(j)|}. \tag{21}$$

The value of 0 for S_m represents the energy flowed through the upper and the lower is equal, in faulty condition, which means both two transistors fail. The positive value for S_m represents the energy flowed through the lower is smaller than that flowed through the upper, which means the lower transistor fails. The negative value for S_m represents the energy flowed through the upper is less than that flowed through the upper-part, which means the upper transistor fails.

Based on the analysis above, a fault diagnostic table is proposed, Table I shows the fault detection and location when ED is used for SM. Where × indicates a do not care condition. The proposed fault-location method includes three steps:

1) identify the fault into three classes by values of SM;
2) identify the broken leg or legs by M_n;
3) identify the broken transitor to the upper or the lower or both of them by S_m.

Taking T1 open-circuit fault for example, $d_{\rm bc} < K_{\rm sim2}$, $d_{\rm ab}, d_{\rm ac} > K_{\rm sim2}$ indicates that leg-a is broken or both leg-b

TABLE II
VALUE RANGES OF THE PARAMETERS

Parameter	K_ξ	K_z	CC,CA $K_{\mathrm{sim}1}$	ED $K_{\mathrm{sim}2}$
Value Range	$0.1-0.4$	$0.07-0.15$	$0.988-0.993$	adaptive

TABLE III
NUMERICAL ANALYSIS OF DIFFERENT SMS WITH EXPERIMENTAL RESULT

Fault	phase to phase	ED	SMs CC	CA
	$(d,\rho,\psi)_{\mathrm{ab}}$	1.00	0.963	0.986
T1	$(d,\rho,\psi)_{\mathrm{bc}}$	0.08	0.994	0.998
	$(d,\rho,\psi)_{\mathrm{ac}}$	1.20	0.962	0.985
	$(d,\rho,\psi)_{\mathrm{ab}}$	6.19	0.829	0.798
T1T2	$(d,\rho,\psi)_{\mathrm{bc}}$	0.60	0.977	0.994
	$(d,\rho,\psi)_{\mathrm{ac}}$	7.25	0.748	0.785
	$(d,\rho,\psi)_{\mathrm{ab}}$	0.36	0.401	0.324
T1T3	$(d,\rho,\psi)_{\mathrm{bc}}$	2.33	0.708	0.738
	$(d,\rho,\psi)_{\mathrm{ac}}$	1.74	0.859	0.742
	$(d,\rho,\psi)_{\mathrm{ab}}$	0.90	0.936	0.946
T1T4	$(d,\rho,\psi)_{\mathrm{bc}}$	3.18	0.951	0.844
	$(d,\rho,\psi)_{\mathrm{ac}}$	3.26	0.871	0.822

and leg-c are broken, $M_a > K_z$ indicates that leg-a is broken, $S_a > 0$ indicates that T1 fails.

E. Tuning Efforts

An important property of any algorithm is low tuning effort, a scheme should work with as little tuning as possible. The proposed fault diagnosis method needs five parameters, including two counter N_1 and N_2, and three criteria K_ξ, K_z, and K_{sim}. N_1 is a mean filter counter to calculate p_1, p_2, N_2 is a counter to avoid close-to-zero oscillation during calculation of p_1, p_2, their values are constant. In fact, only two parameters need tuning in this paper. K_ξ is used as criterion for nearly-zero current sample, defined as (23), where A_m is the current amplitude of phase-m, θ_s is a small constant. Larger value of θ_s will increase the robustness to transient, however, smaller value will reach fast detection. In this paper, the value of θ_s is suggested to set as $\frac{1}{60} \sim \frac{1}{30}$. K_z is a threshold to identify broken leg, close-to-zero current samples percentage in a period is $4\theta_s/2\pi$ in healthy condition considering that there are two ZCSs, so K_z should be larger than $4\theta_s/2\pi$ given as (24). Because the value ranges of CC, CA, and ED are different, the thresholds are different when different SMs are used for CLs after CSA, $K_{\mathrm{sim}1}$ is applied to CC and CA, the value should be closed to 1, $K_{\mathrm{sim}2}$ is applied to ED, it is suggested as (26), where K_0, λ are constants. The large value of λ will increase detection time, the small value will increase robustness, λ is set 4 in this paper. K_0 is set to avoid false alarm in healthy condition when all $d_{\mathrm{ab}}, d_{\mathrm{bc}}, d_{\mathrm{ac}}$ are small, K_0 is set 0.1 in this paper. Effective value ranges for the parameters based on experimental results are showed in Table II, the large tuning ranges of thresholds show high efficiency of the proposed algorithm

$$k_\xi = A_m \sin(\theta_s) \tag{22}$$

$$k_z > 4\frac{\theta_s}{2\pi} \tag{23}$$

$$d_{\max} = \max(d_{\mathrm{ab}}, d_{\mathrm{bc}}, d_{\mathrm{ac}})$$

$$d_{\min} = \min(d_{\mathrm{ab}}, d_{\mathrm{bc}}, d_{\mathrm{ac}})$$

$$K_{\mathrm{sim2}} = \frac{\lambda d_{\min} + d_{\max}}{\lambda + 1}\frac{d_{\max} + d_{\min}}{d_{\max} - d_{\min}} + K_0. \tag{24}$$

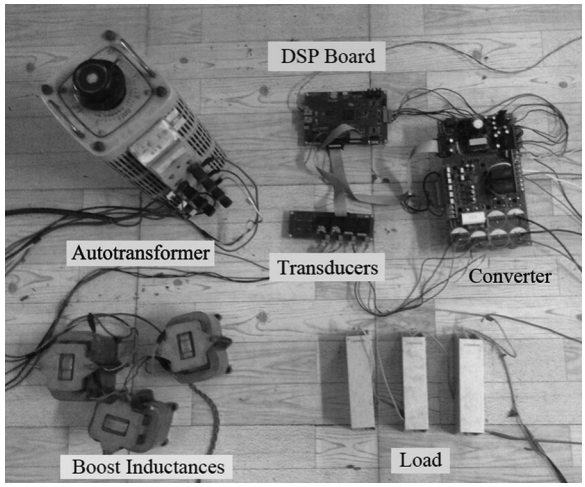

Fig. 5. Experimental setup.

IV. EXPERIMENTAL RESULTS

The following analyses are based entirely on the experimental results since they give a better presentation of the algorithm performance in the presence of nonideal properties, such as model uncertainty, measurements noise, rectifier dead-time effects, etc. Some indices were presented to evaluate the performance of the proposed fault diagnosis method, such as robustness, detection time, etc. Four kinds of faults were investigated, including single open-circuit fault, multiple open-circuit faults in the same leg, multiple open-circuit fault both on the upper or the lower, multiple open-circuit fault one is on the upper and the other one is on the lower, represented by T1, T1T2, T1T3, and T1T4 failure, respectively. All kinds of transistor open-circuit faults were performed by inhibiting their respective gate signals while keeping the bypass diode still connected. The experimental results are presented by the signals FD and FI, which represents the results of fault detection and fault identification.

Three-phase rectifier was implemented in a TMS320F28335 board. The experimental setup is showed in Fig. 5, consists of a control board, a power converter with a switching frequency of 10 kHz, and the IGBT dead time of 3.2 μs, three phase primary voltage source of $80\sqrt{3}$v, primary inductance of 8.6 mH, and resistance load. The parameters $K_\xi, K_z, K_{\mathrm{sim}1}, \lambda\ K_0$ for fault diagnosis were set as $0.2, 0.08, 0.99, 4, 0.1$, respectively, $K_{\mathrm{sim}2}$ is online adaptive.

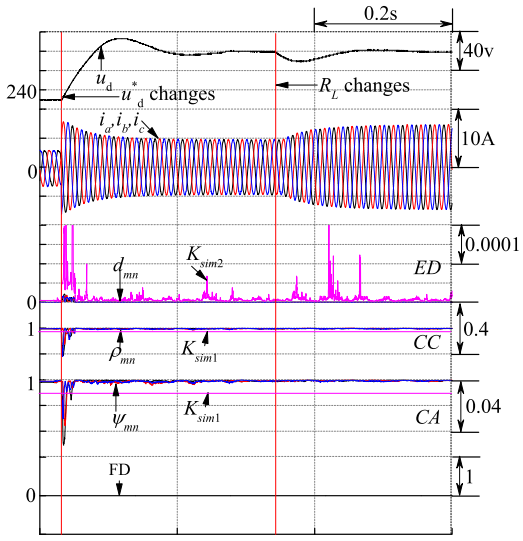

Fig. 6. Experimental results of antitransients, from up to down, output voltage U_d, three-phase currents i_a, i_b, i_c, values of SMs $d_{\rm mn}$, $\rho_{\rm mn}$, $\psi_{\rm mn}$, Diagnostic signal FD.

A. Immunity to an Abrupt Change of Reference DC Value and Resistance Load

Disturbances of load change and reference dc value change are examined to prove the fair robustness of the proposed diagnostic method, showed in Fig. 6. $U_d{}^*$ ranges from 230 to 280 V at 0.035 s and R_L ranges from 120 to 80 Ω at 0.335 s. The output voltage fluctuates during the transients, showed as subfigure 1. Three phase currents are showed as subfigure 2. Values of SMs with ED, CC, and CA are showed as subfigure 3, 4, 5, respectively. From the results, all three SMs are robust to load changes, but they are fluctuating when the reference voltage changes, the fluctuation of CC is nearly 0.4, which leads to a false alarm, the fluctuation of CA is 0.04, showed as subfigure 5, which is over the alert line, ED are all nearly equal to zero, it is far smaller than $K_{\rm sim2}$. No false alarm occurs during transient if ED is adopted as features for fault detection, FD remains zero, showed as subfigure 6.

B. Fault Diagnosis

1) Single Open-Circuit Fault Diagnosis: Fig. 7 shows the diagnostic process when T1 open circuit occurs, from up to low, waveforms of output voltage, three-phase currents, SMs, and diagnostic signals are given out. When the fault occurs, indicated as the red line, output voltage ripple occurs and phase current are distorted, showed as subfigure 1, 2, respectively. In healthy condition, SMs that are applied to measure similarity between any two CLs are equal, when open-circuit fault occurs, SMs are not equal again, fault is detected. After fault occurs, subfigure 3 shows the results when CC is used as SM, $\rho_{\rm ab}$ is larger than $K_{\rm sim1}$, $\rho_{\rm ac}$, $\rho_{\rm bc}$ are equal and both smaller than $K_{\rm sim1}$. Subfigure 4 shows the results when CA is used as SM, $\psi_{\rm bc}$ is larger than $K_{\rm sim1}$, $\psi_{\rm ab}$, $\psi_{\rm ac}$ are equal and both smaller than $K_{\rm sim1}$. Subfigure 5 shows the results when ED is used as SM, $d_{\rm bc}$ is the smallest and $d_{\rm ac}$ is the largest, $d_{\rm bc}$ is smaller than $K_{\rm sim2}$,

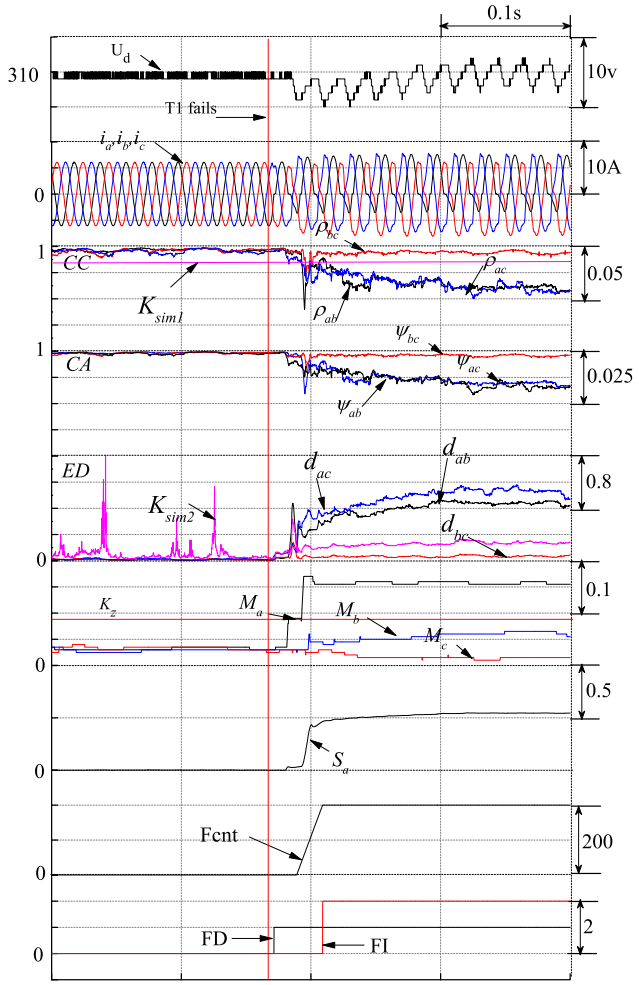

Fig. 7. Fault diagnosis process when T1 fails with reference voltage $U_d{}^* = 310$ V, from up to down, output voltage, three-phase currents, similarity measurements signals, features M_m, S_m and diagnostic signals FD, FI.

$d_{\rm ab}$ and $d_{\rm ac}$ are equal and both larger than $K_{\rm sim2}$. All the results of different SMs show that leg-b and leg-c are symmetrical, and they are asymmetrical with leg-a, which indicates that leg-a is broken or both leg-b and leg-c are broken. The percentages of close-to-zero intervals of three phase currents in a period are showed in subfigure 6, M_a is larger than the K_z, which indicates leg-a is broken.The polar of the energy flowed through the upper and the lower part of the broken leg is positive, showed as subfigure 7, $S_a > 0$, which indicates only the upper transistor is broken. Here, an FI report counter "Fcnt" is introduced to filter out impulse false alarm caused by primary inductance energy release when fault occurs. A delay of L samples is introduced by the counter Fcnt. This delay is very small with only one current fundamental period, if the fault location results keep unchanged, then FI is confirmed. The diagnosis results remain unchanged over a period, showed as subfigure 8, the counter "Fcnt" is equal to L. As a result, open circuit is located to T1. The detection time is 0.005 s, isolation time is 0.026 s. The detection time and location time are both nearly a current period, which proves the proposed method is fast and effective.

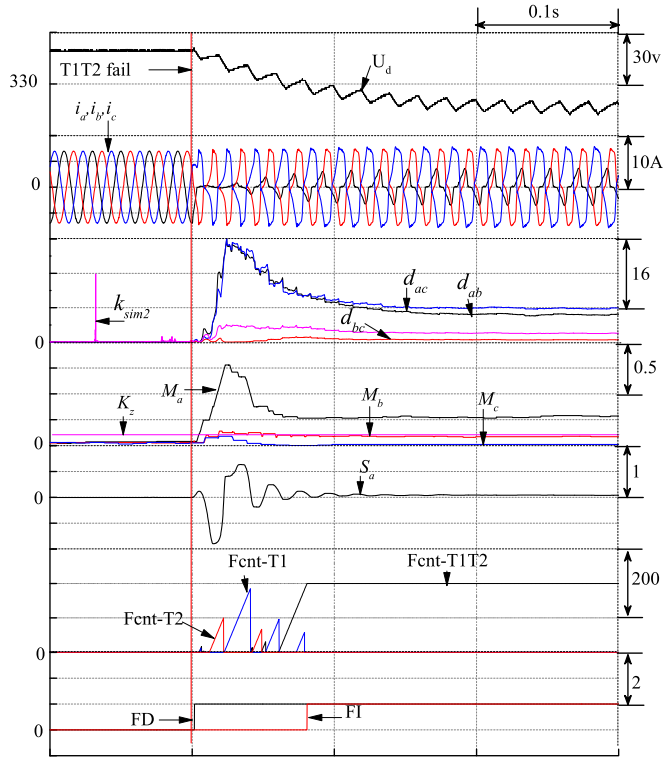

Fig. 8. Fault diagnosis process when T1T2 fails with reference voltage $U_d{}^* = 350$ V, from up to down, output voltage, three-phase currents, similarity measurements signals $d_m\, n$, features M_m , S_m , and diagnostic signals FD, FI.

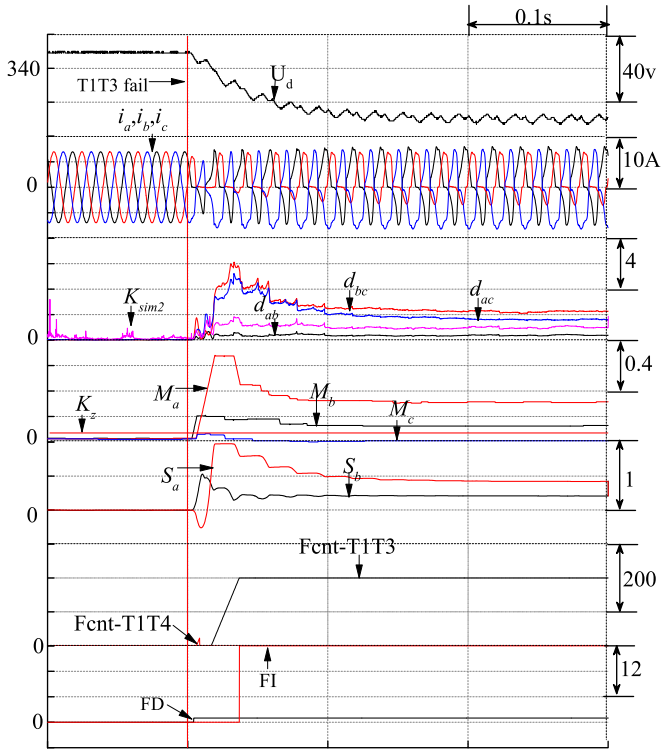

Fig. 9. Fault diagnosis process when T1T3 fails with reference voltage $U_d{}^* = 350$ V, from up to down, output voltage, three-phase currents, similarity measurements signals d_{mn}, features M_m , S_m and diagnostic signals FD, FI.

2) Performance Comparison of Three SMs: Three different SMs are used to analyze the relationship between any two CLs after CSA. In order to confirm the best application, their diagnostic performance is compared from three aspects: false alarm in fault detection, tuning efforts, and efficiency in fault location. First, from the experimental results of transients showed in Fig. 6, both CC and CA will cause false alarms when reference voltage $U_d{}^*$ changes, while no false alarm occurs in ED. Second, threshold K_{sim1} for SM with CC and CA needs tuning, meanwhile, the tuning range is small. While threshold K_{sim2} for SM with Ed is online updating. Third, in order to evaluate the efficiency of three SMs, Table III gives out the experimental results of three SMs in four typical open-circuit faults. The data in the table comes from experimental board, they are the mean values of SMs during ten current periods in faulty condition. Only ED can identify all four typical open-circuit faults. Consequently, only ED is applied to multiple open-circuit fault diagnosis due to its acceptable superiors in both robustness, tuning effort, and efficiency.

3) Multiple Open-Circuit Fault Diagnosis: Fig. 8 shows the diagnostic process when T1T2 are broken, from up to low, waveforms of output voltage, three-phase currents, SMs ,and diagnostic signals are given. When the fault occurs, indicated as the red line, output voltage ripple occurs and phase currents are distorted, showed as subfigure 1, 2, respectively. Values of ED are showed as subfigure 3, $d_{\mathrm{ab}} \approx d_{\mathrm{ac}} \neq d_{\mathrm{bc}}$, fault can be detected. After fault occurs, $d_{\mathrm{ac}} \approx d_{\mathrm{bc}} > K_{\mathrm{sim2}}$, $d_{\mathrm{bc}} < K_{\mathrm{sim2}}$, which indicates leg-$b$, leg-$c$ are symmetrical, and they are asymmetrical with leg-a. Hence, leg-a is broken or both leg-b and leg-c are broken. The percentages of close-to-zero intervals in a period of three phase currents are showed in subfigure 4, M_a is larger than the K_z, which indicates leg-a is broken. The polar of the energy flowed through the upper and the lower part of the broken leg fluctuate near to zero for the energy release of corresponding inductance need a short time, showed as subfigure 5, two single open-circuit faults occur alternatively during this transient, however, the corresponding counters of diagnostic results are smaller than L, they are identified as impulse false alarm. After the phase currents recover stable, counters of diagnostic results for multiple open-circuit fault is equal to L, which indicates both the upper transistor and the lower transistor are broken. As a result, open circuit is located at T1T2.

Experimental results of T1T3 fail and T1T4 fail are presented in Figs. 9 and 10, respectively. All the results show the merit of three phase rectifier open-circuit fault detection and location method based on current similarity analysis.

C. Comparison of Previous Methods

In this section, performance of the proposed diagnostic method is compared with previous methods, such as detection and location time, robustness, tunning efforts, cost, sensitive to system parameters, and efficiency, the results are showed in Table IV. The proposed method can detect and locate single open-circuit fault within 1 current fundamental period,

TABLE IV
COMPARISON WITH PREVIOUS METHODS

Diagnostic Method	Detection Time	Robustness	Tuning Efforts	Cost	Sensitive to System Parameters	Efficiency
Current angle-based method [32]	$1/4$cycle	Low	Medium	Low	Low	Single
Modified Park's vector method [33]	$>$ 2cycles	Low	High	Low	Low	Single
Model-based method [19]	$1/4$cycle	High	Medium	Low	High	Single and multiple
Proposed method	$1/4$ cycle	High	Medium	Low	Low	Single and Multiple

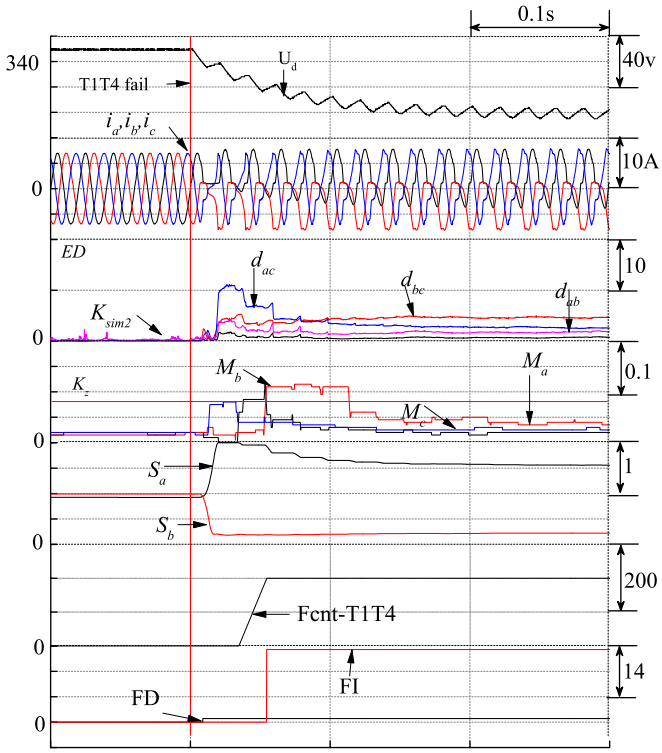

Fig. 10. Fault diagnosis process when T1T4 fails at with reference voltage $U_d{}^* = 350$ V, from up to down, output voltage, three-phase currents, similarity measurements signals d_{mn}, features M_m , S_m and diagnostic signals FD, FI.

meanwhile it is robust to load and reference changes, moreover, it can identify 21 open-circuit faults without any extra sensors or electrical circuits. As can be seen in Table IV, the proposed method can achieve good performance in the indexes mentioned above, while the previous methods have one or more shortcomings.

V. CONCLUSION

A single and multiple open-circuit fault diagnosis method in three-phase rectifier has been proposed based on similarity analysis of CLs after CSA. CDR is proposed to eliminate the phase difference among three phase CLs. Derivative-based CSA is applied to solve the shifting, scaling, and time warpings in reconstructed CLs. Three SMs are designed and their performances are compared, such as robustness, tuning, and efficiency, ED performs best. The proposed fault detection method is based on the symmetrical analysis, fault can be detected when values of ED are not equal again. The proposed fault-location method includes three steps, the fault is first divided into three classes by the values of SMs, then identified to broken legs by M_n, finally located to broken transistor by S_a.

The proposed fault diagnosis method is robust to transients, fast and low cost without extra sensors or electrical circuits. It has potential application to transistor open circuit in matrix, two-level, and multilevel converters.

REFERENCES

[1] B. L. Dokić and B. Blanuša, *Power Electronics Converters and Regulators*, 3rd ed. New York, NY, USA: Springer, 2015.
[2] V. Smet *et al.*, "Ageing and failure modes of IGBT modules in high-temperature power cycling," *IEEE Trans. Ind. Electron.*, vol. 58, no. 10, pp. 4931–4941, Oct. 2011.
[3] S. Yang, D. Xiang, A. Bryant, P. Mawby, L. Ran, and P. Tavner, "Condition monitoring for device reliability in power electronic converters: A review," *IEEE Trans. Power Electron.*, vol. 25, no. 11, pp. 2734–2752, Nov. 2010.
[4] S. Nandi, H. Toliyat, and X. Li, "Condition monitoring and fault diagnosis of electrical motors-a review," *IEEE Trans. Energy Convers.*, vol. 20, no. 4, pp. 719–729, Dec. 2005.
[5] S. Yang, A. Bryant, P. Mawby, D. Xiang, L. Ran, and P. Tavner, "An industry-based survey of reliability in power electronic converters," *IEEE Trans. Ind. Appl.*, vol. 47, no. 3, pp. 1441–1451, May/Jun. 2011.
[6] B. Lu and S. K. Sharma, "A literature review of IGBT fault diagnostic and protection methods for power inverters," *IEEE Trans. Ind. Appl.*, vol. 45, no. 5, pp. 1770–1777, Sep./Oct. 2009.
[7] H. Renaudineau, J.-P. Martin, B. Nahid-Mobarakeh, and S. Pierfederici, "Dc–dc converters dynamic modeling with state observer-based parameter estimation," *IEEE Trans. Power Electron.*, vol. 30, no. 6, pp. 3356–3363, Jun. 2015.
[8] B. Li, S. Shi, B. Wang, G. Wang, W. Wang, and D. Xu, "Fault diagnosis and tolerant control of single igbt open-circuit failure in modular multilevel converters," *IEEE Trans. Power Electron.*, vol. 31, no. 4, pp. 3165–3176, Apr. 2016.
[9] M. A. Rodríguez-Blanco, A. Va zquez Pe rez, L. Herna ndez Gonza lez, V. Golikov, J. Aguayo-Alquicira, and M. May-Alarcon, "Fault detection for IGBT using adaptive thresholds during the turn-on transient," *IEEE Trans. Ind. Electron.*, vol. 62, no. 3, pp. 1975–1983, Mar. 2015.
[10] F. Zidani, D. Diallo, M. E. H. Benbouzid, and R. Naït-Saïd, "A fuzzy-based approach for the diagnosis of fault modes in a voltage-fed PWM inverter induction motor drive," *IEEE Trans. Ind. Electron.*, vol. 55, no. 2, pp. 586–593, Feb. 2008.
[11] Z. Gao, C. Cecati, and S. X. Ding, "A survey of fault diagnosis and fault-tolerant techniques—Part i: Fault diagnosis with model-based and signal-based approaches," *IEEE Trans. Ind. Electron.*, vol. 62, no. 6, pp. 3757–3767, Jun. 2015.
[12] Z. Gao, C. Cecati, and S. Ding, "A survey of fault diagnosis and fault-tolerant techniques—Part ii: Fault diagnosis with knowledge-based and hybrid/active approaches," *IEEE Trans. Ind. Electron.*, vol. 62, no. 6, pp. 3768–3774, Jun. 2015.
[13] Q. An, L. Sun, L. Sun, and T. M. Jahns, "Low-cost diagnostic method for open-switch faults in inverters," *Electron. Lett.*, vol. 46, no. 14, pp. 1021–1022, 2010.
[14] Q.-T. An, L.-Z. Sun, K. Zhao, and L. Sun, "Switching function model-based fast-diagnostic method of open-switch faults in inverters without sensors," *IEEE Trans. Power Electron.*, vol. 26, no. 1, pp. 119–126, Jan. 2011.
[15] R. de Araujo Ribeiro, C. Jacobina, E. Cabral da Silva, and A. Lima, "Fault detection of open-switch damage in voltage-fed PWM motor drive

systems," *IEEE Trans. Power Electron.*, vol. 18, no. 2, pp. 587–593, Mar. 2003.
[16] A. Mendes, A. Cardoso, and E. Saraiva, "Voltage source inverter fault diagnosis in variable speed AC drives, by park's vector approach," in *Proc. 7th Int. Conf. Power Electron. Variable Speed Drives (Conf. Publ. No. 456)*, 1998, pp. 538–543.
[17] K. Rothenhagen and F. Fuchs, "Performance of diagnosis methods for IGBT open circuit faults in three phase voltage source inverters for AC variable speed drives," presented at the *European Conf. Power Electronics Applications.*, Dresden, Germany, 2005.
[18] K. Rothenhagen and F. W. Fuchs, "Performance of diagnosis methods for IGBT open circuit faults in voltage source active rectifiers," in *Proc. IEEE 35th Annu. Power Electron. Spec. Conf.*, 2004, vol. 6., pp. 4348–4354.
[19] I. Jlassi, J. O. Estima, E. Khil, S. Khojet, N. M. Bellaaj, and A. J. Marques Cardoso, "Multiple open-circuit faults diagnosis in back-to-back converters of PMSG drives for wind turbine systems," *IEEE Trans. Power Electron.*, vol. 30, no. 5, pp. 2689–2702, May 2015.
[20] S.-M. Jung, J.-S. Park, H.-W. Kim, K.-Y. Cho, and M.-J. Youn, "An MRAS-based diagnosis of open-circuit fault in PWM voltage-source inverters for PM synchronous motor drive systems," *IEEE Trans. Power Electron.*, vol. 28, no. 5, pp. 2514–2526, May 2013.
[21] D. R. Espinoza-Trejo, D. U. Campos-Delgado, G. Bossio, E. Bárcenas, J. E. Hernández-Díez, and L. F. Lugo-Cordero, "Fault diagnosis scheme for open-circuit faults in field-oriented control induction motor drives," *IET Power Electron.*, vol. 6, no. 5, pp. 869–877, 2013.
[22] W. Sleszynski, J. Nieznanski, and A. Cichowski, "Open-transistor fault diagnostics in voltage-source inverters by analyzing the load currents," *IEEE Trans. Ind. Electron.*, vol. 56, no. 11, pp. 4681–4688, Nov. 2009.
[23] J. Zhang, J. Zhao, D. Zhou, and C. Huang, "High-performance fault diagnosis in PWM voltage-source inverters for vector-controlled induction motor drives," *IEEE Trans. Power Electron.*, vol. 29, no. 11, pp. 6087–6099, Nov. 2014.
[24] F. Wu and J. Zhao, "A real-time multiple open-circuit fault diagnosis method in voltage-source-inverter fed vector controlled drives," *IEEE Trans. Power Electron.*, vol. 31, no. 2, pp. 1425–1437, Feb. 2016.
[25] C. Brunson, L. Empringham, L. De Lillo, P. Wheeler, and J. Clare, "Open-circuit fault detection and diagnosis in matrix converters," *IEEE Trans. Power Electron.*, vol. 30, no. 5, pp. 2840–2847, May 2015.
[26] U.-M. Choi, H.-G. Jeong, K.-B. Lee, and F. Blaabjerg, "Method for detecting an open-switch fault in a grid-connected NPC inverter system," *IEEE Trans. Power Electron.*, vol. 27, no. 6, pp. 2726–2739, Jun. 2012.
[27] U.-M. Choi and K.-B. Lee, "Detection method of an open-switch fault and fault-tolerant strategy for a grid-connected t-type three-level inverter system," in *Pro. IEEE Energy Convers. Congr. Expo.*, 2012, pp. 4188–4195.
[28] J.-S. Lee and K.-B. Lee, "An open-switch fault detection method and tolerance controls based on SVM in a grid-connected t-type rectifier with unity power factor," *IEEE Trans. Ind. Electron.*, vol. 61, no. 12, pp. 7092–7104, Dec. 2014.
[29] W. Wang, A. C. f. Liu, H. S. h. Chung, R. W. h. Lau, J. Zhang, and A. W. l. Lo, "Fault diagnostic device for photovoltaic panels," in *Proc. IEEE Appl. Power Electron. Conf. Expo.*, Mar. 2015, pp. 2609–2616.
[30] L. M. Caseiro and A. Mendes, "Real-time IGBT open-circuit fault diagnosis in three-level neutral-point-clamped voltage-source rectifiers based on instant voltage error," *IEEE Trans. Ind. Electron.*, vol. 62, no. 3, pp. 1669–1678, Mar. 2015.
[31] B. Gou, X. Ge, S. Wang, X. Feng, J. B. Kuo, and T. G. Habetler, "An open-switch fault diagnosis method for single-phase PWM rectifier using a model-based approach in high-speed railway electrical traction drive system," *IEEE Trans. Power Electron.*, vol. 31, no. 5, pp. 3816–3826, May 2016.
[32] W.-S. Im, J.-M. Kim, D.-C. Lee, and K.-B. Lee, "Diagnosis and fault-tolerant control of three-phase AC–DC PWM converter systems," *IEEE Trans. Ind. Appl.*, vol. 49, no. 4, pp. 1539–1547, Jul./Aug. 2013.
[33] W.-S. Im, J.-S. Kim, J.-M. Kim, D.-C. Lee, and K.-B. Lee, "Diagnosis methods for IGBT open switch fault applied to 3-phase aC/DC PWM converter," *J. Power Electron.*, vol. 12, no. 1, pp. 120–127, 2012.
[34] S. Khomfoi, W. Sae-Kok, and I. Ngamroo, "An open circuit fault diagnostic technique in IGBTs for AC to DC converters applied in microgrid applications," *J. Power Electron.*, vol. 11, no. 6, pp. 801–810, 2011.
[35] S. Casey and N. Reingold, "Self-similar fractal sets: Theory and procedure," *IEEE Comput. Graph. Appl.*, vol. 14, no. 3, pp. 73–82, May 1994.
[36] Y. Chen, M. Nascimento, B. C. Ooi, and A. K. Tung, "SpADe: On shape-based pattern detection in streaming time series," in *Proc. IEEE 23rd Int. Conf. Data Eng.*, 2007, pp. 786–795.
[37] F.-P. Chan, A.-C. Fu, and C. Yu, "Haar wavelets for efficient similarity search of time-series: with and without time warping," *IEEE Trans. Knowl. Data Eng.*, vol. 15, no. 3, pp. 686–705, 2003.
[38] E. Keogh and S. Kasetty, "On the need for time series data mining benchmarks: A survey and empirical demonstration," *Data Mining Knowl. Discovery*, vol. 7, no. 4, pp. 349–371, 2003.

Feng Wu (S'15) was born in Hubei Province, China, in 1990. He received the B.S. degree in automation control from Department of Control Science and Engineering, Huazhong University of Science and Technology (HUST), Wuhan, China, in 2013. He is currently working toward the Ph.D. degree in control theory and control engineering at the School of Automation.

His research interests include power electronics, high performance ac motor drives, fault diagnosis, and reliability design.

Jin Zhao (M'14–SM'14) was born in Hubei Province, China, in 1967. He received the B.S. and Ph.D degrees in control theory and control engineering from the Department of Control Science and Engineering, Huazhong University of Science and Technology (HUST), Wuhan, China, in 1989 and 1994, respectively.

Since 2004, he has been a Full Professor with the School of Automation, HUST. During 2001–2002, he was a Visiting Scholar in the Power Electronics Research Laboratory, University of Tennessee, Knoxville. His research interests include power electronics, electrical drives, fault diagnosis, and intelligent control. He is the author or coauthor of more than 100 technical papers.